



Efficient Separation of Xylene Isomers by a Robust Calcium-Based Metal-Organic Framework through Synergetic Thermodynamically and Kinetically Controlled Mechanism

Journal:	<i>Journal of Materials Chemistry A</i>
Manuscript ID	TA-ART-09-2021-008055.R1
Article Type:	Paper
Date Submitted by the Author:	27-Oct-2021
Complete List of Authors:	<p>Lin, Yuhan; Shenzhen Polytechnic Zhang, Jian; Shenzhen Polytechnic, Hoffmann Institute of Advanced Materials, Postdoctoral Innovation Practice Base Pandey, Haardik; Wake Forest University, Physics Dong, Xinglong; King Abdullah University of Science and Technology, Advanced Membranes and Porous Materials Centre, Division of Chemical and Life Science and Engineering Gong, Qihan; Petrochina Petrochemical Research Institute Wang, Hao; Shenzhen Polytechnic, Hoffmann Institute of Advanced Materials Yu, Liang ; South China University of Technology, School of Chemistry and Chemical Engineering Zhou, Kang; Shenzhen Polytechnic Yu, Wei; Shenzhen Polytechnic Huang, Xiaoxi; Shenzhen Polytechnic, Hoffmann Institute of Advanced Materials Thonhauser, Timo; Wake Forest University, Department of Physics Han, Yu; King Abdullah University of Science and Technology, Advanced Membranes and Porous Materials Centre, Division of Chemical and Life Science and Engineering Li, Jing; Rutgers The State University of New Jersey, Chemistry and Chemical Biology</p>

ARTICLE

Efficient Separation of Xylene Isomers by a Robust Calcium-Based Metal-Organic Framework through Synergetic Thermodynamically and Kinetically Controlled Mechanism

Received 00th January 20xx,
Accepted 00th January 20xx

DOI: 10.1039/x0xx00000x

Yuhan Lin,^{‡a} Jian Zhang,^{‡a} Haardik Pandey,^{‡b} Xinglong Dong,^c Qihan Gong,^d Hao Wang,^{*a} Liang Yu,^a Kang Zhou,^a Wei Yu,^a Xiaoxi Huang,^a Timo Thonhauser,^b Yu Han,^{*c} and Jing Li^{*e,a}

Adsorptive separation of physically and chemically similar molecules and understanding the underlying host-guest interactions at molecular level are of significant scientific and practical importance. Here we report the development of a novel calcium-based metal-organic framework, formulated as $\text{Ca}_3(\text{Htcpp})_2$ ($\text{Htcpp} = 2,3,5,6$ -tetrakis(4-carboxyphenyl)-pyrazine) featuring microporosity and high stability. This compound shows distinct adsorption behavior toward xylene isomers and is capable of separating them efficiently at industrially relevant temperature. The selective adsorption is attributed to a synergetic thermodynamic and kinetic effect. The host-guest interactions were probed directly by single-crystal X-ray diffraction analysis and the adsorption affinity was evaluated through computational molecular simulations.

Introduction

Adsorptive separation of highly similar hydrocarbon molecules is considered as a challenging yet promising alternative technology to traditional distillations, due to the lower energy cost and reduced carbon dioxide emission associated with this technology. It is, therefore, of great industrial importance.¹ Xylene isomers, particularly o-xylene and m-xylene, are of the highest level of separation complexity as a result of their extremely similar physical and chemical properties. The boiling point, polarizability and dipole moment of the three isomers, p-xylene, m-xylene, and o-xylene (denoted as pX, mX, and oX, respectively), follows the sequence of $\text{oX} > \text{mX} \approx \text{pX}$, but the differences are minimal. Shape-selective adsorption has been realized by certain adsorbents, including zeolites and metal-organic frameworks (MOFs), for the separation of pX from mX and oX, by taking advantage of the relatively slim geometry of pX and its smaller kinetic diameter (5.8 Å for pX vs 6.8 Å for mX and oX).²

Compared to traditional inorganic and organic adsorbents, MOFs are intrinsically advantageous for the separation of physically similar molecules, including xylene isomers, because of their diverse structures and tunable pore size/shape.³ Zhang et al. reported a MOF, $\text{Cu}_2(\text{pypz})_2$ ($\text{Hypyz} = 4$ -(1H-pyrazol-4-yl)pyridine), with tunable structural flexibility.⁴ It selectively adsorbs pX over mX and oX with a selectivity as high as 51. Zhu et al. developed a microporous MOF, $\text{In}(\text{OH})(\text{OBA})$ ($\text{H}_2\text{OBA} = 4,4'$ -oxybis(benzoic acid)), which adsorbs pX only but fully excludes mX and oX, acting as a molecular sieve.⁵ The separation of mX and oX is more challenging because of their similar shape and size. Zaworotko et al. reported a flexible MOF, sql-1-Co-NCS , that can discriminate between mX and oX owing to their different gate-opening pressure, with oX as the preferentially adsorbed isomer.⁶ Selective adsorption of oX over mX has also been observed for $\text{Co}_2(\text{dobdc})$, $\text{Co}_2(\text{m-dobdc})$,⁷ $\text{MIL-53}(\text{Cr})$,⁸ CD-MOF-1 ,⁹ and the recently reported ZU-61 .¹⁰ Preferential adsorption of oX in these materials could be attributed to its higher polarizability and dipole moment, leading to higher adsorption affinity to MOFs. Comparatively, MOFs showing selective adsorption of mX over oX are relatively rare. Yang and Schröder et al. recently reported the separation of xylene isomers by the $\text{MFM-300}(\text{M})$ ($\text{M} = \text{In}, \text{V}, \text{Fe}, \text{Al}$) family, which exhibit adsorption preference following the sequence of $\text{mX} > \text{oX} > \text{pX}$ as a result of cooperative supramolecular binding interactions.¹¹ In this work we report a new microporous calcium-based MOF, $\text{Ca}_3(\text{Htcpp})_2$ (denoted as HIAM-201 , HIAM refers to Hoffmann Institute of Advanced Materials), that demonstrates efficient separation of xylene isomers with adsorption preference sequence of $\text{pX} > \text{mX} > \text{oX}$. Its pX/mX , pX/oX , and mX/oX selectivities are as high as 4.2, 24.4, and 5.8, respectively, attributed to a combined thermodynamic and kinetic effect.

^a Hoffmann Institute of Advanced Materials, Shenzhen Polytechnic, 7098 Liuxian Boulevard, Shenzhen, Guangdong 518055, P. R. China
E-mail: wanghao@szpt.edu.cn

^b Department of Physics and Center for Functional Materials, Wake Forest University, Winston-Salem, NC 27109, USA

^c Advanced Membranes and Porous Materials Center, Physical Sciences and Engineering Division, King Abdullah University of Science and Technology Thuwal 23955-6900, Saudi Arabia
E-mail: yu.han@kaust.edu.sa

^d Fundamental Science & Advanced Technology Lab, PetroChina Petrochemical Research Institute, Beijing 102200, P. R. China

^e Department of Chemistry and Chemical Biology, Rutgers University, 123 Bevier Road, Piscataway, New Jersey 08854, United States
E-mail: jingli@rutgers.edu

[‡]These authors contributed equally to this work.

Electronic Supplementary Information (ESI) available: [details of any supplementary information available should be included here]. See DOI: 10.1039/x0xx00000x

Results and discussion

Calcium-based MOFs (Ca-MOFs) are advantageous for adsorption related applications because of their gravimetric benefit and relatively high stability. However, Most of the reported Ca-MOFs feature low-dimensional structures, or high-dimensional dense structures. Three-dimensional (3D) Ca-MOFs with permanent porosity are relatively rare (Table S1).¹² Here, HIAM-201 was synthesized via solvothermal reactions of CaCl₂ and H₄tcpp in ethanol at 120 °C for 2 days, which yielded block-shaped colourless crystals (See Supporting Information for synthesis details). Single-crystal X-ray diffraction analysis revealed the compound crystallizes in triclinic crystal system with a space group of $P\bar{1}$. Ca²⁺ ions are either 6- or 7-coordinated with octahedral or pentagonal bipyramid geometry. It is noteworthy that the Ca²⁺ metal centres are coordinated exclusively to carboxylates from H₄tcpp and no coordinated solvents are observed. This is relatively rare for Ca-MOFs as

water/solvent molecules tend to occupy one or more coordination sites of Ca²⁺ as a result of its high hydration energy.¹² The structure of HIAM-201 is built on one-dimensional (1D) [Ca₃(COOH)₂(COO)₆]_n chains, which are interconnected by organic linkers to form the final 3D structure with a **deh1** topology (Fig. 1 and Fig. S1).¹³ Three out of four carboxylates in each H₄tcpp linker are deprotonated, with one remaining undeprotonated, but all four carboxylates are coordinated to Ca²⁺ centers. The structure possesses 1D open channels along both *a* and *b* axis, with a diameter of ~6.5 Å (H-H, excluding vdW radii). It should be mentioned that the structure of HIAM-201 is totally different from Ca(H₂tcpb) built on H₄tcpb (H₄tcpb = 2,3,5,6-tetrakis(4-carboxyphenyl)-benzene), which is similar to H₄tcpp but with a benzene core instead of pyrazine.¹⁴ Unlike H₂tcpb²⁻ which adopts a planar configuration when rigidified in Ca(H₂tcpb), H₄tcpp³⁻ is no longer planar in the crystal structure of HIAM-201 (Fig. S2).

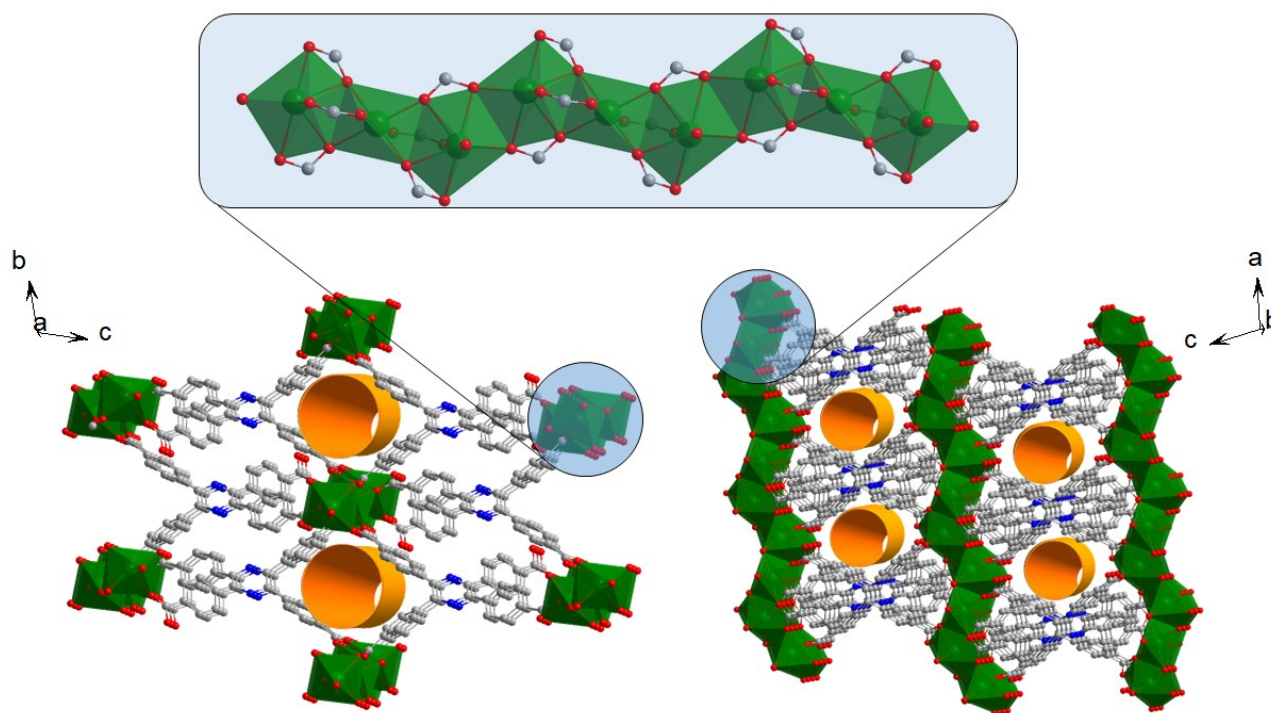


Fig. 1. 3D crystal structure of HIAM-201 showing 1D open channels along *a* axis and *b* axis, and the 1D inorganic chain. Ca: green polyhedra, O: red, N: blue, C: grey, Hydrogen atoms are omitted for clarity.

The porosity of HIAM-201 was studied by N₂ adsorption at 77 K. The compound can be activated by direct heating at 150 °C. It shows a Type I adsorption profile for N₂ with a saturated capacity of 159 cc/g, yielding a BET surface area of 604 m²/g and a pore volume of 0.24 cm³/g (Fig. S3). The surface area of HIAM-201 is among the highest for Ca-MOFs, only slightly lower than that of Ca-BTB (Table S1).¹⁵ DFT pore size distribution analysis reveals the compound has a uniform pore size of 6-7 Å, consistent with the value measured from its crystal structure (Fig. S4).

Ca-MOFs, particularly those without coordinated solvents, generally feature robust structures because of the high charge density of calcium metal which leads to strong, ionic-like bonds with organic linkers. We thus examined the stability of the title compound under various conditions. As expected, the material kept intact after being exposed to open air at 250 °C for a week, indicating its high thermal stability and exceptional resistance to moisture (Fig. S5). Thermogravimetric analysis (TGA) displayed a plateau up to 400 °C before a notable weight loss associated to structural decomposition and the TGA curve of

the activated HIAM-201 revealed that no notable weight loss was observed before 400 °C (Fig. S6). In addition, the synthesis of HIAM-201 can be easily scaled up by 10 times in lab reactions and the product retains the same crystallinity as that of the small-scale reactions (Fig. S8).

The robust framework, high surface area, and suitable pore dimensions of HIAM-201 encouraged us to explore its capability as an adsorbent for separation of xylene isomers. We selected xylene isomers because their molecular dimensions, particularly those of oX and mX, are close to the pore size of the MOF. Adsorption isotherms of xylene isomers were collected at 120–150 °C, the temperatures relevant to industrial processes (Fig. 2a–c). Interestingly, HIAM-201 exhibit different adsorption behavior toward the three xylene isomers. For pX, the adsorption isotherms at different temperatures followed the same trend and the adsorbed amount decreased slightly as a function of increasing temperature (Fig. 2a). In contrast, the

adsorption profiles for mX and oX are distinctly different for the same temperature range. Notable decreases in uptake amounts were observed for mX and oX when temperature increased from 120 °C to 150 °C. A comparison of the adsorption isotherms of xylenes at 150 °C suggests that HIAM-201 exhibits a noticeable adsorption preference for pX over the other two isomers (Fig. 2d). The adsorption capacity of pX was 126.7 mg/g at 150 °C and 1.2 kPa, notably higher than that for mX (61.1 mg/g) and oX (33.8 mg/g) under identical conditions. Henry constants, which are commonly applied to evaluate gas-solid interactions, were calculated based on the adsorption isotherms at different temperature (Table S2). In general, Henry constants followed the trend of pX > mX > oX. For example, Henry constants of pX, mX, and oX were calculated to be 299.0, 61.0, and 24.3 mg/g/kPa at 150 °C, respectively, indicating a descending order of interaction with the MOF.

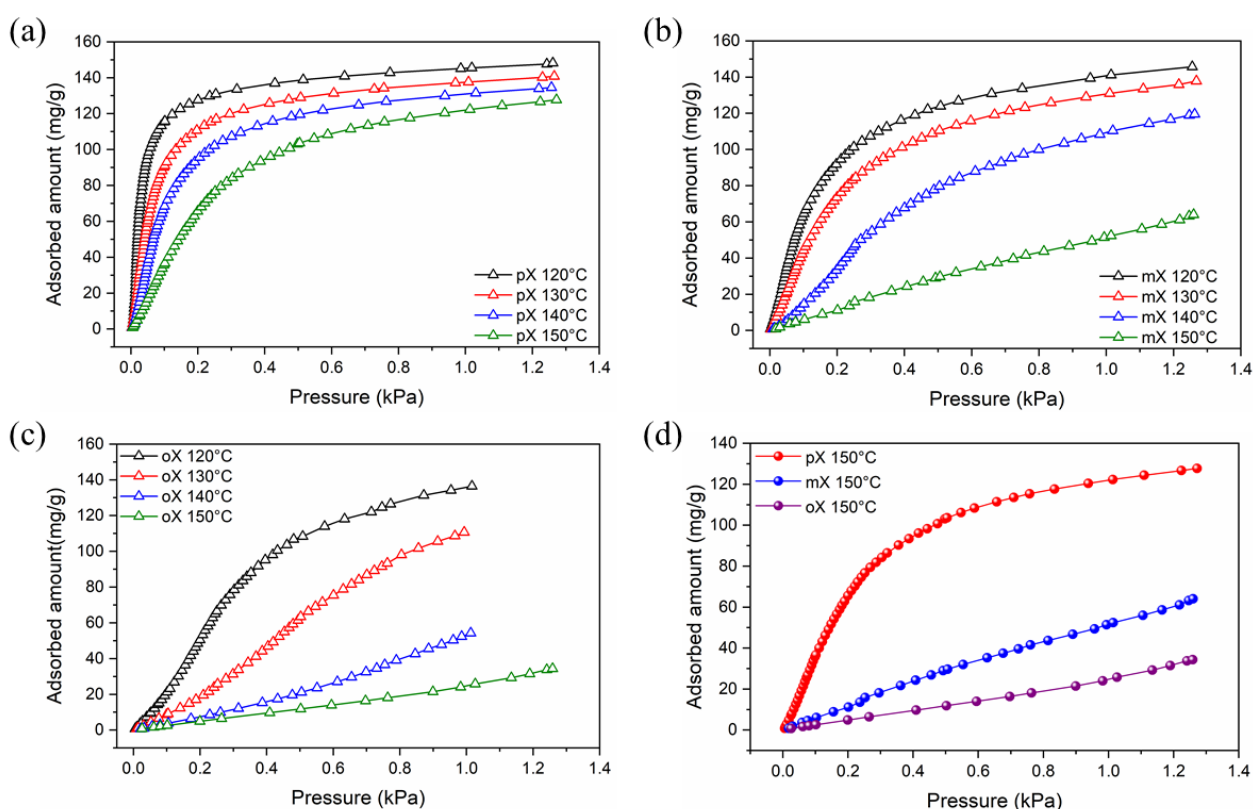


Fig. 2. (a–c) Adsorption isotherms of pX (a), mX (b), oX (c) at 120–150 °C. (d) Comparison of adsorption isotherms of pX, mX, and oX at 150 °C.

In light of the comparable dimensions of the channels of HIAM-201 and xylene isomers, we also investigated the adsorption kinetics (Fig. S9) with a home-modified gravimetric adsorption analyser (See Supporting Information for experimental details). At 120 °C and 0.8 kPa, the ratio of their diffusion rate coefficients, $D(\text{pX})/D(\text{mX})/D(\text{oX})$, is 1.89/1.24/1.0, following the same trend of their Henry constants. These results indicated that the sequence of adsorption preference by HIAM-201 (pX > mX > oX) observed from the adsorption isotherms, is a result of the synergetic effect of thermodynamics and kinetics.

To explore the stability of HIAM-201 towards repeated adsorption-desorption cycles, 10 consecutive adsorption-desorption cycles were carried out at 150 °C between 0.8 kPa pX vapour and nitrogen. No noticeable loss of adsorption capacity was observed during the 10 cycles (Fig. S10), suggesting robustness of the framework. IR spectra of pristine HIAM-201 and HIAM-201 loaded with different xylene isomers have been collected (Fig. S11), which suggested no notable changes. PXRD patterns (Fig. S12) of HIAM-201 loaded with different xylene isomers revealed the overall structure was

retained upon loading of different guest molecules. A shift to lower angle of the doublet peak at around $2\theta = 8^\circ$ has been observed for xylenes loaded HIAM-201, which is consistent with their corresponding simulated patterns.

The differences in adsorption capacity and adsorption kinetics of xylene isomers by HIAM-201 suggests that the material may potentially be useful for the separation of these physically and chemically similar molecules. We thus evaluated its separation capability through multicomponent column breakthrough measurements at 150 °C. An equimolar ternary vapor mixture of pX, mX, and oX was passed through a column packed with activated HIAM-201 and the eluted vapor was subject to gas chromatography (GC) analysis. The breakthrough curves are presented in Fig. 3a, which exhibit a clear separation of the three isomers. The first isomer eluted out was oX, which broke out at the 13th minute, followed by mX at the 55th minute. In contrast, pX was retained in the column for the longest time,

and was not detected at the outlet until the 130th minute. The elution sequence of the three isomers are consistent with their adsorption preference by HIAM-201. We calculated the dynamic adsorption selectivities based on the ratios of adsorption capacity of each isomer before breakthrough. The pX/mX, pX/oX, and mX/oX selectivities were 2.45, 10.47, and 4.27, respectively. The values, in particular pX/oX and mX/oX selectivities, are notably higher than most of the reported adsorbents, including the recently reported benchmark materials MFM-300 (Fig. S13).¹⁰⁻¹¹ The high adsorption selectivities of HIAM-201 should be attributed to its combined thermodynamically and kinetically controlled effects toward the adsorption of xylene isomers. Three consecutive runs of breakthrough experiments revealed the separation capability of the material was well retained, indicating once again its high stability with respect to adsorption-regeneration cycles.

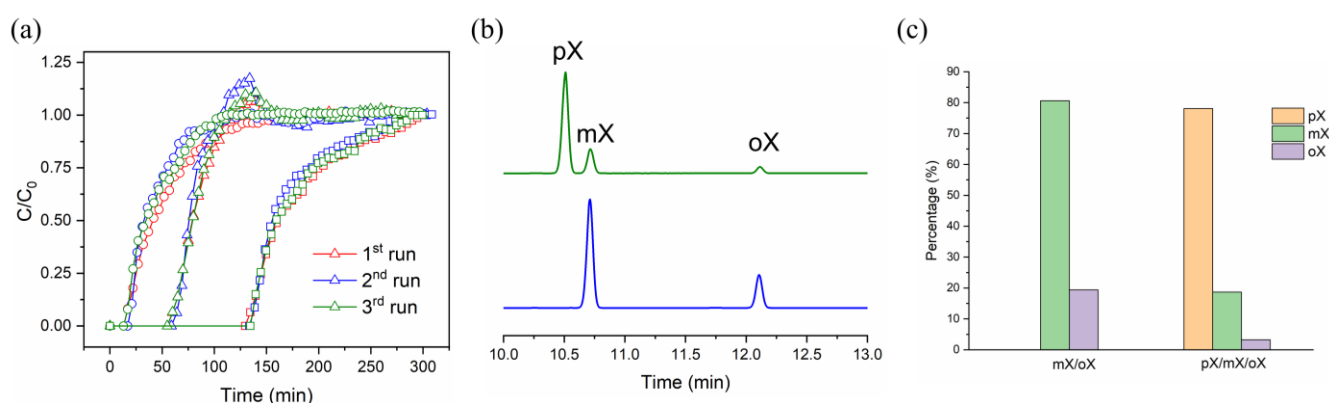


Fig. 3. Separation of xylene mixtures by HIAM-201. (a) Breakthrough curves of the three consecutive runs of multicomponent column breakthrough experiments for xylene isomers at 150 °C, squares: pX, triangles: mX, cycles: oX. (b) GC analysis of desorbed xylenes from HIAM-201 saturated with equimolar xylene vapors (Blue: mX/oX; Green: pX/mX/oX) at 150 °C. (c) Integration of GC peaks.

To further evaluate the capability of HIAM-201 for the separation of xylene mixtures, we examined the composition of xylenes adsorbed in the pores of the MOF after the adsorption equilibrium was reached. The experiments were carried out using the foregoing gravimetric adsorption analyser used to evaluate the adsorption kinetics. Activated HIAM-201 was exposed to an equimolar ternary pX/oX/mX vapor mixture with a partial pressure of 0.8 kPa (carried by nitrogen) at 150 °C until adsorption equilibrium was reached. Desorption was performed by immersing the xylenes loaded MOF sample in *n*-hexane under stirring. The subsequently filtered solution was subject to GC analysis (Fig. 3b-c). The results suggested that the pX/mX, pX/oX, and mX/oX selectivities were 4.17, 24.25, and 5.80, respectively. The selectivities followed the same trend of that observed in breakthrough experiments, but with higher values. This could be attributed to the fact that the adsorbed oX and mX may be substituted by the more favored pX when approaching sufficient equilibrium, leading to higher adsorption selectivities. To evaluate how HIAM-201 would perform in separating mX and oX, a parallel experiment was carried out

with an equimolar binary mixture of mX and oX as a feed instead of the ternary mixture. Following identical procedures, the mX/oX selectivity was calculated to be 4.16, indicating the notable preference of mX over oX and its capability for the separation of the two isomers.

Preferential adsorption of mX over oX by MOFs was rarely observed in previous studies because of their similar molecular geometries and kinetic diameters. The high mX/oX adsorption selectivity by HIAM-201 should be attributed to the higher adsorption affinity and adsorption rate of the former. To further understand the adsorption preference of mX over oX, computational simulations (See Supporting Information for details) were performed to evaluate their binding energies with the framework. Two adsorption sites were identified for both mX and oX in the channels of HIAM-201 (Fig. S14), and the binding energy calculations performed at both sites indicated that mX has a stronger binding with the framework as compared to oX. The highest binding energies of the two isomers occur at different sites within the MOF. The mX binds strongest at site-1 (channels along the *a* axis) with binding

energy of 115.05 kJ/mol and oX has the highest binding energy of 108.87 kJ/mol at site-2 (channels along the *b* axis). The difference in binding energies further explained why the adsorption of mX is more favored over oX by HIAM-201.

To explore the guest-MOF interactions at molecular level, we attempted to obtain the crystal structures of HIAM-201 loaded with xylenes. Thorough guest exchange of ethanol, the initial solvents residing in the pores of HIAM-201, by pX (or mX, oX) afforded pX (or mX, oX) loaded HIAM-201, denoted as pX@HIAM-201 (or mX@HIAM-201, oX@HIAM-201). The crystal structures of xylenes loaded HIAM-201 were determined through single-crystal X-ray diffraction (Fig. S15-S17). Taking pX@HIAM-201 as an example, pX molecules were adsorbed in both channels along *a* and *b* axis (Fig. 4), interacting with the framework via Van der Waals forces. The closest H...H and C...C distances between pX and the framework are 2.14 and 3.27 Å, respectively, indicating notable guest-host interactions. The other two isomers, mX and oX, reside at positions similar to that of pX, packing with certain disorders (Fig. S16-S17). The guest-host vdW interaction is similar for different xylene isomers. The difference in adsorption affinity could be attributed to the degree of matching between the shape of xylene molecules and the channel shape of HIAM-201.

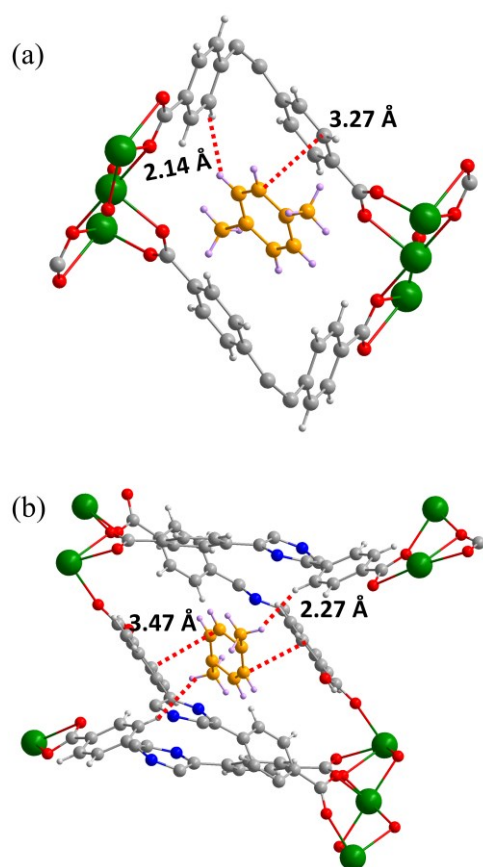


Fig. 4. Adsorption sites of pX in the channel along *a* axis (a) and channel along *b* axis (b) of HIAM-201, determined by single-crystal X-ray diffraction.

Conclusions

Adsorptive separation of xylene isomers, in particular mX and oX with similar molecular geometry and dimension, is challenging but industrially important. It has stringent requirement with respect to the pore structure of the adsorbents. We in this work present a new calcium-based microporous MOF, HIAM-201, with optimal pore size and shape for the separation of xylene isomers. Its adsorption preference follows the sequence of pX > mX > oX, with high adsorption selectivities evidenced by multicomponent adsorption studies. Our studies reveal that the high adsorption selectivities are results of synergetic effects of thermodynamics and kinetics.

Author Contributions

H.W., Y.H., and J. L. Conceived the idea. Y. L., L. Y., K. Z., and W. Y. performed the synthesis, characterization, single-component adsorption study, and structure determination. J. Z., X. D., Q. G., and X. H. performed the column breakthrough and GC analysis. H. P. and T. T. carried out the computational calculations. H. W. wrote the paper and all authors contributed to the discussion and final proof of the manuscript.

Conflicts of interest

There are no conflicts to declare.

Acknowledgements

We thank the National Natural Science Foundation of China (21901166), Guangdong Natural Science Foundation (2019A1515010692), and Shenzhen Science and Technology Program (No. JCYJ20190809145615620, RCYX20200714114539243). Work in the US was entirely supported by the U.S. Department of Energy, Office of Science, Office of Basic Energy Sciences under Award No. DE-SC0019902.

Notes and references

‡Crystal data files are accessible through CCDC data base with CCDC Numbers of 2093140-2093143.

1. R. Lively, *Nature*, 2016, **532**, 435-437.
2. J.-R. Li, R. J. Kuppler and H.-C. Zhou, *Chem. Soc. Rev.*, 2009, **38**, 1477-1504.
3. (a) H. Furukawa, K. E. Cordova, M. O'Keeffe and O. M. Yaghi, *Science*, 2013, **341**, 1230444; (b) H. Wang, Y. Liu and J. Li, *Adv. Mater.*, 2020, **32**, 2002603; (c) Z. Bao, G. Chang, H. Xing, R. Krishna, Q. Ren and B. Chen, *Energy Environ. Sci.*, 2016, **9**, 3612-3641; (d) K. Adil, Y. Belmabkhout, R. S. Pillai, A. Cadiau, P. M. Bhatt, A. H. Assen, G. Maurin and M. Eddaoudi, *Chem. Soc. Rev.*, 2017, **46**, 3402-3430.
4. X. Yang, H.-L. Zhou, C.-T. He, Z.-W. Mo, J.-W. Ye, X.-M. Chen and J.-P. Zhang, *Research*, 2019, **2019**, 9463719.
5. Z. Jin, H.-Y. Zhao, X.-J. Zhao, Q.-R. Fang, J. R. Long and G.-S. Zhu, *Chem. Commun.*, 2010, **46**, 8612-8614.

6. S.-Q. Wang, S. Mukherjee, E. Patyk-Kaźmierczak, S. Darwish, A. Bajpai, Q.-Y. Yang and M. J. Zaworotko, *Angew. Chem. Int. Ed.*, 2019, **58**, 6630-6634.
7. M. I. Gonzalez, M. T. Kapelewski, E. D. Bloch, P. J. Milner, D. A. Reed, M. R. Hudson, J. A. Mason, G. Barin, C. M. Brown and J. R. Long, *J. Am. Chem. Soc.*, 2018, **140**, 3412-3422.
8. (a) Z. He, Y. Yang, P. Bai and X. Guo, *J. Ind. Eng. Chem.*, 2019, **77**, 262-272; (b) R. E. Osta, A. Carlin-Sinclair, N. Guillou, R. Walton, F. Vermoortele, M. Maes, D. Vos and F. Millange, *Chem. Mater.*, 2012, **24**, 2781-2791.
9. L. Chen, D.-D. Zhu, G.-J. Ji, S. Yuan, J.-F. Qian, M.-Y. He, Q. Chen and Z.-H. Zhang, *J. Chem. Technol. Biot.*, 2018, **93**, 2898-2905.
10. X. Cui, Z. Niu, C. Shan, L. Yang, J. Hu, Q. Wang, P. C. Lan, Y. Li, L. Wojtas, S. Ma and H. Xing, *Nat. Commun.*, 2020, **11**, 5456.
11. X. Li, J. Wang, N. Bai, X. Zhang, X. Han, I. da Silva, C. G. Morris, S. Xu, D. M. Wilary, Y. Sun, Y. Cheng, C. A. Murray, C. C. Tang, M. D. Frogley, G. Cinque, T. Lowe, H. Zhang, A. J. Ramirez-Cuesta, K. M. Thomas, L. W. Bolton, S. Yang and M. Schröder, *Nat. Commun.*, 2020, **11**, 4280.
12. S. Xian, Y. Lin, H. Wang and J. Li, *Small*, 2021, **17**, 2005165.
13. J.-P. Mo, F. Bigdeli, Y. Ying, C.-Q. Zhu, M. Zhu, Y.-S. Li, X.-H. Li, H.-P. Xiao, A. Morsali and A. Ramazani, *Polyhedron*, 2019, **158**, 144-153.
14. (a) H. Wang, X. Dong, E. Velasco, D. H. Olson, Y. Han and J. Li, *Energy Environ. Sci.*, 2018, **11**, 1226-1231; (b) X. Chen, A. M. Plonka, D. Banerjee, R. Krishna, H. T. Schaef, S. Ghose, P. K. Thallapally and J. B. Parise, *J. Am. Chem. Soc.*, 2015, **137**, 7007-7010.
15. K. Noh, N. Ko, H. J. Park, S. Park and J. Kim, *Crystengcomm*, 2014, **16**, 8664-8668.